N C A R Manuscript No. 64

Pre-publication review copy

The dynamical influence of topography on the large-scale motion of the atmosphere

by

Akira Kasahara

August 1965

NATIONAL CENTER FOR ATMOSPHERIC RESEARCH

Boulder, Colorado

ABSTRACT

In an attempt to understand the dynamical influence of the earth's topography upon the large-scale motion of the atmosphere, the system of "shallow water" equations on the rotating earth is integrated numerically. The model consists of an incompressible, homogeneous, hydrostatic and inviscid fluid. The "beta-plane" approximation is used to simplify the model. The fluid is confined in a channel bounded by two parallel "walls" extended to the west and east directions. Periodic boundary conditions are applied to simulate the cyclic continuity of the channel in the longitude. A circular obstacle of parabolic shape is placed at the bottom in the middle of the channel. The steady-state solutions in the absence of the obstacle are used as the initial conditions of the problem. Five different cases are investigated in detail. All computations were performed up to 20 days (some cases were run longer) with a time step of 6 minutes.

The following main results were obtained: (1) Westerly flows past the obstacle produced a train of long waves on the lee side, which can be identified as "planetary" waves. On the other hand, easterly flows are little disturbed by the obstacle and long waves do not appear; (2) The number of waves produced in the westerly cases agrees with the number expected from the steady-state Rossby-

Haurwitz wave formula for various intensities of the zonal flow past the obstacle.

The results of the present calculations are compared favourably with those obtained in the early 1950's by Fultz, Long and Frenzen in the laboratory experiments of the flow past a barrier in a rotating hemispherical shell. Finally, a theoretical consideration was given to explain characteristic differences between westerly and easterly flows past the obstacle observed in the numerical experiments.

I. Introduction

It has been recognized that the earth's atmosphere is influenced by the condition of the earth's surface. As far as the large-scale motion in the atmosphere is concerned, its influence appears to depend upon (1) the distribution of continents and oceans and (2) the large-scale topography of the earth's surface. The first factor may appear as a thermal influence upon the motion due to the temperature contrast between the air over the lands and the air over the seas. The second factor, on the other hand, may be considered as a dynamical nature.

It was discussed by Charney and Eliassen (1949), Bolin (1950) and others (see References) that mountain barriers of the size of the Himalayas and the Rockies play an important role in determining the positions of the semi-permanent high-level troughs and ridges in the westerlies. Their argument is based on the observation that certain basic characteristics of the flow patterns at upper levels in the northern hemisphere do not change essentially from summer to winter, in spite of the reversal in the thermal contrast between the continents and oceans.

In an attempt to understand the dynamical influence of mountain barriers upon the atmospheric flow patterns in a more direct way, a series of laboratory experiments were conducted at the University of Chicago (Hydrodynamic Laboratory) by Fultz and Long (1951), Long

(1952), Fultz and Frenzen (1955) and Frenzen (1955). They investigated nearly two-dimensional motions of homogeneous fluid around obstacles in a rotating hemispherical shell using the apparatus shown in Figure 1. The equipment consists of two concentric hemispheres of mean radius 10 cm, rotating together about a vertical axis. The distance between the shells is about 1.6 cm and the space is filled with water up to the "equator." Figure 2 shows a cross section of the spheres with the position of the obstacle. To produce the effect of a zonal current moving past the obstacle, the obstacle was moved through the fluid. The motion of the obstacle was accomplished by attaching it, by a thin arm, to a shaft within the one used to rotate the spheres. Rotating the obstacle more slowly than the spheres generates a relative westerly flow past it, while rotating it more rapidly generates a relative easterly flow. Observations were made through a rotoscope, a reversing prism mounted with its optical axis along the common axis of rotation of the shells. With this device, all motions of tracer particles in the fluid were seen relative to the framework determined by the rotation rate of the prism.

Figure 3 shows two schematic sketches of the flow patterns observed relative to the obstacle. The left picture shows the pattern in the case of westerly flow and the right picture shows the pattern in the case of easterly flow. Long (1952) describes

that "the most striking features of the flow in the presence of this obstacle are as follows: when a westerly current flows past the obstacle, the fluid goes into a series of oscillations, extending around the whole globe, . . . An easterly current, however, does not oscillate and is little disturbed by the obstacle, . . ."

In this study, a set of three partial differential equations which govern the motion of fluid past an obstacle is integrated numerically under prescribed initial and boundary conditions. It is hoped that such a numerical experiment would aid in our understanding of the dynamical effect of large-scale topography upon the motion of the atmosphere. We are concerned with finite-amplitude and time dependent motions rather than small-amplitude and steady-state motions as considered by most of the previous investigators on this subject. Asai and Nitta (1963) have attempted a numerical integration of the primitive equations for a barotropic model including topography, but they have not integrated the equations long enough to demonstrate clearly the effects of topography upon the atmospheric flow patterns.

2. Basic equations and boundary conditions

We consider an incompressible, homogeneous, hydrostatic and inviscid atmosphere. The motion of this fluid may be described by the following well-known "shallow water" equations,

$$\frac{\partial u}{\partial t} + u\frac{\partial u}{\partial x} + v\frac{\partial u}{\partial y} = -g\frac{\partial h}{\partial x} + fv \qquad (2.1)$$

$$\frac{\partial v}{\partial t} + u\frac{\partial v}{\partial x} + v\frac{\partial v}{\partial y} = -g\frac{\partial h}{\partial y} - fu \qquad (2.2)$$

$$\frac{\partial h}{\partial t} + \frac{\partial}{\partial x}\{u(h-H)\} + \frac{\partial}{\partial y}\{v(h-H)\} = 0. \qquad (2.3)$$

The two space variables x and y are cartesian coordinates directing toward the east and the north, respectively. The x-y plane is the "beta-plane," namely the Coriolis parameter f, representing $2\omega \sin\theta$, with ω denoting the angular velocity of the earth and θ the latitude, is a function of y only. In (2.1) - (2.3), u, v denote the x, y components of the fluid velocity; h is the height of the free surface of the fluid; H is the height of an obstacle which is a function of both x and y; and g denotes the acceleration due to gravity and t, time.

Figure 4(a) shows the domain of integration for (2.1) - (2.3) which is a fixed rectangular region with sides parallel to the coordinate axes. The northern and southern boundaries are "solid" walls. The flow is periodic in the east-west direction with a period equal to the distance L between the east and west boundaries. A circular obstacle is placed at the bottom in the middle of the domain. As seen in Figure 4(b), which is a cross section view of

the flow, the bottom is flat outside of the mountain region. The top of the fluid is a free surface.

In summary, the boundary conditions for (2.1) to (2.3) of the problem are prescribed so that: (1) the y-component of the velocity vanishes for all time along the northern and southern boundaries; (2) u, v and h are periodic in the space variable x with a period equal to the distance between the east and west boundaries.

3. Initial conditions

It is well-known that, in the absence of mountains, Eqs. (2.1) to (2.3) possess the following stationary solutions

$$u = \bar{u} \quad (= \text{constant})$$
$$v = 0 \tag{3.1a}$$

and $\partial \bar{h}/\partial x = 0$ and $\partial \bar{h}/\partial y = -f\bar{u}/g$ or by integrating the last equation with respect to y, we have

$$h(y) = h_0 - \frac{\bar{u}}{g}\int_0^y f\, dy \tag{3.1b}$$

where h_0 denotes the value of h at $y = 0$.

We are going to use (3.1) as the initial conditions of the problem in the presence of mountains. This means that the wind field and the pressure field are not balanced initially over the mountain regions. Therefore, one expects oscillations to be generated in the fluid. We can show, however, that the disturbances created in

that way by the mountain are quasi-geostrophic in nature so long as the slope of the mountain remains in the order of 10^{-3}, as pointed out by Gambo (1957) and Phillips (1963). The following simple scale analysis is slightly different from the arguments presented by them but will demonstrate the same point in question.

By differentiating (2.1) and (2.2) with y and x, respectively, and using (2.3), the following well-known potential vorticity equation is obtained.

$$\frac{1}{\zeta+f}\frac{d}{dt}(\zeta+f) = \frac{1}{h-H}\left[\frac{dh}{dt} - \frac{dH}{dt}\right] \tag{3.2}$$

where d/dt signifies the material derivative. If we consider a stationary quasi-geostrophic motion, the contribution from the first term on the right-hand side of (3.2) is negligible. Therefore, the time rate of change in the magnitude of the absolute vorticity should balance approximately with the time rate of stretching of the fluid column due to the effect of flow passing over the mountains. The order of magnitude of the left-hand side term may be approximated by $V\beta/f$ where $\beta = \partial f/\partial y$ and V denotes the characteristic flow speed. The order of magnitude of the divergence generated by the mountain is $V|\nabla H|/h$ where $|\nabla H|$ denotes the characteristic slope of the mountain. By equating those

two terms above, we obtain

$$\beta / f = |\nabla H| / h$$

or

$$|\nabla H| = \frac{h}{a} \cot\theta \tag{3.3}$$

where a is a mean radius of the earth (= 6370 km). Table 1 shows the critical slope of the "geostrophic" mountain given by (3.3) at different latitudes for a mean height of the atmosphere h = 8 km.

Table 1. Critical slope of "geostrophic" mountain, in unit of 10^{-3}

θ (°N)	20	30	40	50	60	70	80
$\lvert\nabla H\rvert$	3.45	2.18	1.50	1.05	0.725	0.457	0.221

It is seen from Table 1 that with the exception of some parts of the Himalayas and Andes, the large-scale topography on the earth induces only the amount of divergence comparable to that of quasi-geostrophic motions. It is, therefore, reasonable to expect that the use of the stationary solutions (3.1) as the initial conditions of the problem in the presence of mountains generates quasi-geostrophic motions rather than inertia-gravity motions which are characterized by a large amount of divergence in the flow.

4. Difference equations

For the purpose of numerical integrations, it is convenient to rewrite Eqs. (2.1) to (2.3) in divergence form, i.e.

$$\frac{\partial U}{\partial t} + \frac{\partial F}{\partial x} + \frac{\partial G}{\partial y} = Q \tag{4.1}$$

where

$$U = \begin{pmatrix} m \\ n \\ \varphi \end{pmatrix} \qquad F = \begin{pmatrix} \frac{m^2}{\varphi} + g\frac{\varphi^2}{2} \\ \frac{mn}{\varphi} \\ m \end{pmatrix}$$

$$G = \begin{pmatrix} \frac{mn}{\varphi} \\ \frac{n^2}{\varphi} + g\frac{\varphi^2}{2} \\ n \end{pmatrix} \qquad Q = \begin{pmatrix} -g\varphi H_x + fn \\ -g\varphi H_y - fm \\ 0 \end{pmatrix} \tag{4.2}$$

and

$$m = u(h-H), \quad n = v(h-H), \quad \varphi = h-H.$$

Here, m and n denote the x and y components of the specific momentum, φ is the thickness of the fluid above the mountain.

The two-step Lax-Wendroff integration scheme proposed by Richtmyer (1963) is applied to (4.1). In order to write down the difference equations, we abbreviate any function $p(x, y, t)$ of $x = j\Delta x$, $y = k\Delta y$ and $t = l\Delta t$ as p^l_{jk} where j, k and l are integers; Δx, Δy and Δt are, respectively, space and time increments. The two-step difference equations for (4.1) consist of the following two schemes which are used at alternate time cycles:

$$1)\quad U_{jk}^{\ell+1} = \bar{U}_{jk}^{\ell} - \frac{1}{2}\left[\lambda \Delta_x F_{jk}^{\ell} + \mu \Delta_y G_{jk}^{\ell}\right] + \tilde{Q}_{jk}^{\ell+\frac{1}{2}}$$

(4.3)

$$2)\quad U_{jk}^{\ell+2} = U_{jk}^{\ell} - \left[\lambda \Delta_x F_{jk}^{\ell+1} + \mu \Delta_y G_{jk}^{\ell+1}\right] + Q_{jk}^{\ell+1}$$

where

$$\lambda = \Delta t / \Delta x \quad , \quad \mu = \Delta t / \Delta y$$

$$\Delta_x F_{jk}^{\ell} = F_{j+1\,k}^{\ell} - F_{j-1\,k}^{\ell}$$

$$\Delta_y G_{jk}^{\ell} = G_{j\,k+1}^{\ell} - G_{j\,k-1}^{\ell}$$

in which F_{jk}^{ℓ} and G_{jk}^{ℓ} are an abbreviation for $F(U_{jk}^{\ell})$ and $G(U_{jk}^{\ell})$;

$$\tilde{Q}_{jk}^{\ell+\frac{1}{2}} = \begin{pmatrix} -\frac{g}{2}\left(\bar{\varphi}_{jk}^{x\ell} + \bar{\varphi}_{jk}^{x\,\ell+1}\right)\lambda \Delta_x H + \frac{f^*}{2}\left(\bar{\eta}_{jk}^{\ell} + \eta_{jk}^{\ell+1}\right) \\ -\frac{g}{2}\left(\bar{\varphi}_{jk}^{y\ell} + \bar{\varphi}_{jk}^{y\ell+1}\right)\mu \Delta_y H - \frac{f^*}{2}\left(\bar{m}_{jk}^{\ell} + m_{jk}^{\ell+1}\right) \\ 0 \end{pmatrix}$$

with

$$f^* = f \Delta t \ ,$$

$$\bar{\varphi}^{x\ell}_{jk} = \frac{1}{2}\left(\varphi^{\ell}_{j+1\,k} + \varphi^{\ell}_{j-1\,k}\right)$$

$$\bar{\varphi}^{y\ell}_{jk} = \frac{1}{2}\left(\varphi^{\ell}_{j\,k+1} + \varphi^{\ell}_{j\,k-1}\right)$$

$$\bar{\varphi}^{\ell}_{jk} = \frac{1}{2}\left(\bar{\varphi}^{x\ell}_{jk} + \bar{\varphi}^{y\ell}_{jk}\right)$$

and similarly for $\bar{n}^{\ell}_{jk}$ and $\bar{m}^{\ell}_{jk}$.

Due to the fact that $\tilde{Q}^{\ell+\frac{1}{2}}$ contains terms at $\ell+1$ time step, the first scheme in (4.3) looks as though it is an implicit procedure. However, if the prediction of $\varphi^{\ell+1}$ (the third component of U) is done first, then the prediction of the first and second components $m^{\ell+1}$ and $n^{\ell+1}$, can be made explicitly by solving the prediction equations for $m^{\ell+1}$ and $n^{\ell+1}$ simultaneously.

If the Q term in (4.3) is ignored, one can show that the combination of the first and second schemes is convergent as Δt and ΔS (in the case of $\Delta x = \Delta y = \Delta S$) approach to zero, if

$$\frac{\Delta t}{\Delta S}\left(|\vec{V}| + \sqrt{g\bar{h}}\right) < \frac{1}{\sqrt{2}} \tag{4.4}$$

where $|\vec{V}|$ is the magnitude of the largest possible flow velocity and $\bar{h}$ is the maximum height of the free surface in the fluid (see Richtmyer, 1963). Stability of the two-step Lax-Wendroff scheme including the Coriolis term should be referred to an article by Houghton, Kasahara and Washington (1965).

Special treatments are made at the northern and southern boundaries. There, the y-component of the velocity v must vanish for all time, but the x-component of the velocity u and the height h are computed from (4.3). In those equations, $\Delta_x F$ is evaluated using the centered difference but $\Delta_y G$ is approximated by the first-order uncentered difference using the grid values on the boundary and the point next to the boundary point at the same x-coordinate in the integration domain. The accuracy of this type of boundary condition can be improved by using a higher-order uncentered differencing. We have tried the use of the second-order boundary condition for a similar problem satisfactorily, and the second-order boundary condition seems to produce a better result than the first-order boundary condition (as it should be!). However, for a long-term integration, the computations with the second-order boundary condition tend to be more unstable than those with the first-order condition, in the sense that purturbations on the boundaries sometimes grow with respect to time, though very slowly. It seems that the use of the first-order condition is not only satisfactory from the standpoint of accuracy, but also is more stable, computationally.

5. Numerical data for computations

The integration domain is a rectangular lattice of equal grid intervals $\Delta X = \Delta y = \Delta S$. The sides have lengths of L and W

in the x and y directions, respectively. The origin of the x and y coordinates is taken at the center of the domain.

The form of mountain studied here is circular and parabolic which is expressed by

$$H(x,y) = H_m\,(1 - R^2/b^2) \qquad \text{for } 0 \le R \le b$$

$$= 0 \qquad \text{for } b < R$$

where

$$b = 4.5\,\Delta S \quad , \quad R^2 = x^2 + y^2,$$

H_m : the maximum height of the obstacle.

The following numerical values for the parameters in the problem are used.

$$\begin{aligned} L &= 72\,\Delta S \\ W &= 18\,\Delta S \\ \Delta S &= (2\pi a \cos 45^\circ)/72 = 393.073 \text{ km} \\ a &= \text{mean radius of earth} = 6370 \text{ km} \\ g &= 9.8 \text{ m/sec}^2 \\ H_m &= 2000 \text{ m} \\ h_o &= 7000 \text{ m} \\ \bar{u} &= \text{a variable constant whose value is different for the different cases to be discussed in the next section.} \end{aligned} \tag{5.1}$$

The time step Δt = 360 sec was chosen to satisfy the stability condition (4.4). All five cases are computed up to 20 days or 4800 time iterations. (Some cases have been computed even longer.)

6. Results of five cases

Case A. Constant f, $\bar{u} = 20$ m/sec.

To investigate the effect of the latitudinal variation of the Coriolis parameter, in this run we fixed the value of the Coriolis parameter as the value at 45^{o}N (= 1.0284×10^{-5} sec^{-1}). The contour patterns of the height deviation from the initial height field are shown in Figure 5 in a series of four figures taken at 2, 8, 14 and 20 days. In each figure the abscissa shows the east-west direction and the ordinate the north-south direction. The circular obstacle is shown by a circle. The initial wind field is a westerly flow of velocity 20 m/sec. The contours are drawn every 50-meter interval. The dashed contours indicate the positive deviation of height and solid contours the negative deviation. The heavy solid contours denote zero lines.

At the beginning the flow past the barrier was modified such that the height of the free surface increases on the windward side of the mountain and decreases on the lee as seen in the top figure. This initial phase of the height distortion appears to be common in

all five cases. However, the subsequent development of the flow patterns becomes quite different, depending upon the intensity of the initial zonal flow and the latitudinal variation of the Coriolis parameter.

It appears that the large depression on the lee has a transient character and moves around the channel with a nearly constant speed of a little less than 20 m/sec. On the other hand, the elevation on the windward side has a stationary character and must therefore be induced by the forcing due to the mountain. It is of interest to note that when the traveling low hits the stationary high, as seen in the fourth figure, it simply lowers the intensity of the stationary high, but then the traveling low eventually moves out of the region without much altering the pattern of the stationary high over the mountain.

Case B. Variable f, $\bar{u} = 20$ m/sec.

In the rest of four cases, the Coriolis parameter f is expressed as

$$f = 2\omega \sin\left\{\frac{\pi}{180}\left(45 + \frac{y}{d}\right)\right\}$$

where d = 111,111 meters. Now let us see the effect of taking into account the latitudinal variation of the Coriolis parameter in the model for the same initial zonal flow of $\bar{u}$ = 20 m/sec, as in Case A. Of course the initial height field is not identical to the one in Case A owing to the latitudinal variation of the Coriolis parameter, but the difference is rather small to be significant in this case.

Figure 6 shows the contour patterns of the height deviation as seen in Figure 5. At first glance, it is noticed that the evolution of the patterns in Case B is remarkably different from that in Case A. The intensities of the high and the low, after two days from the start in this case, are stronger than those in Case A.

It may be worthwhile to point out that at least the early phase of the evolution of the flow patterns may be explained in the following manner from the conservation equation of the potential vorticity (3.2); namely

$$\frac{d}{dt}\left[\frac{\zeta+f}{h-H}\right] = 0. \tag{6.1}$$

As the flow currents go over the barrier from the <u>west</u>, the thickness of the flow $h-H$ must decrease, and therefore the absolute vorticity $\zeta+f$ must also decrease. The decrease of the absolute vorticity tends to deflect the flow toward <u>lower</u> latitudes. However as the flow moves to lower latitudes, the flow experiences the decrease of the earth's vorticity, f . Therefore the reduction of the relative vorticity becomes less or it may even increase as the flow moves continuously southeastwards. The increase of relative vorticity tends to deflect the flow toward higher latitudes. Repeating the decrease and increase of the relative vorticity sets up the

generation of waves appearing on the lee side as the sequence of eddies. It is evident that the latitudinal variation of the Coriolis parameter is essential in the process of the formation of this type of long waves which are identified as the planetary waves as discovered by C. G. Rossby and Collaborators (1939). It is not likely that the flow patterns eventually settle to an exact steady state, though the number of waves, which is in between 3 to 4, appears to be unchanged after two or three weeks.

Case C. Variable f, $\bar{u} = -20$ m/sec.

Let us now see what happens in the case of an easterly flow. Figure 7 shows the evolution of the height deviation field of this case. The initial phase, as seen in the top figure, is similar to the ones observed in the westerly cases with the exception of direction of the flow. The depression on the lee moves out from the area of the obstacle, just as it did in Case A. However, the intensity of the depression eventually fades out and the elevation over the obstacle remains. It is a remarkable feature of the easterly case that the obstacle does not generate oscillations and the intensity of the elevation over the obstacle is weak. These findings agree very well, qualitatively, with those observed in the laboratory experiments described in the Introduction. It is instructive to apply again the conservation equation of the potential vorticity (6.1) to demonstrate characteristics of the flow patterns of easterlies past the obstacle.

As the flow currents go over the obstacle from the east, the thickness of the flow $h-H$ decreases, and therefore the absolute vorticity $\zeta + f$ must also decrease. The decrease of the absolute vorticity tends to deflect the flow toward higher latitudes. However as the flow moves to higher latitudes, the flow experiences the increase of the earth's vorticity, f .Therefore, the relative vorticity must reduce further and the flow will turn more clockwise. Eventually, the flow will move to lower latitudes and the anticyclonic curvature of the flow will be reduced. The shape of the flow is therefore likely to be a loop and the generation of waves is not likely in the case of easterlies.

Case D. Variable f, $\bar{u}$ = 40 m/sec.

We shall come back to westerly flow cases again. To investigate the dependence of the number of waves generated by the obstacle upon the intensity of the initial zonal current, we take the case of westerly flow with $\bar{u} =$ 40 m/sec. Figure 8 shows the evolution of the height deviation field similar to the one shown in Figure 6. A major difference between the results of Case B and Case D is that the number of waves generated in this case is clearly 2. The result suggests, therefore, that the number of waves decreases as the intensity of the zonal current increases and vice versa. To prove the latter point, the following case was run.

Case E. Variable f, $\bar{u}$ = 8 m/sec.

In this case, the intensity of the initial westerly flow was reduced to 8 m/sec. Figure 9 shows the result of this case. The first three figures are for the height deviation and the last figure shows the pattern of the y-component of the velocity at 20 days. It is seen that the system of highs and lows generated by the obstacle tends to be localized in this weak westerly flow case, and it is not clear, at least in the height deviation fields, how many waves are generated. However, it is seen from the fourth figure which shows the pattern of the y-component of velocity, that the number of waves may be somewhere around 5 to 6.

7. Theoretical considerations

In this section, we shall attempt to give some explanations for several unique features in the numerical results described in the last section. As we mentioned in section 3, the flows generated by the obstacle are quasi-geostrophic in character. We can, therefore, approximate the velocity field $\mathbb{V}$ in terms of the height field h with the use of the geostrophic wind relationship $\mathbb{V} = -\frac{g}{f}\mathbb{K} \times \nabla h$, where $\mathbb{K}$ is the vertical unit vector. We shall consider small amplitude perturbations superimposed on a constant zonal current $\bar{u}$. With these as assumptions, we obtain the following linear equation for the perturbation height h :

$$\frac{\partial}{\partial t}(\nabla^2-\lambda^2)h + \bar{u}\frac{\partial}{\partial x}(\nabla^2-\lambda^2)h + (\beta+\lambda^2\bar{u})\frac{\partial h}{\partial x} = -\lambda^2\bar{u}\frac{\partial H}{\partial x} \tag{7.1}$$

where $\nabla^2 = \partial^2/\partial x^2 + \partial^2/\partial y^2$, $\lambda^2 = f_o^2/(gh_o)$.

A solution which is proportional to $\cos my \cdot \exp\{ik(x-ct)\}$ satisfies both the boundary condition (the y-component of geostrophic wind vanishes along the northern and southern boundaries) and the homogeneous part of (7.1), if the phase velocity C satisfies the following frequency equation

$$C = \bar{u} - \frac{\beta+\lambda^2\bar{u}}{k^2+m^2+\lambda^2} \tag{7.2}$$

which is known as the Rossby-Haurwitz wave formula (see Rossby and Collaborators, 1939 ; Rossby, 1949; and Haurwitz, 1940a). In (7.2), $m = \pi/L_y$ and $k = 2\pi/L_x$ where L_y is the half wavelength of the disturbance in the y-direction and L_x is the full wavelength in the x-direction. As we have seen in the evolution of height deviation fields, only a single mode predominates in the y-direction in most cases. Therefore, we shall assume that L_y is equal to the width of the channel W . In the x-direction, let us denote L_x to be L/ℓ where L is the length of the channel between the east and west boundaries and then ℓ becomes the number of waves appearing in the channel.

If we ask for the stationary state $C = 0$ in (7.2), we can find the relationship between $\bar{u}$ and ℓ for given values of L, W and latitude, θ. Expressing β to be $\frac{2\omega}{a}\cos\theta$ where a is a mean radius of the earth, the stationary condition of (7.2) can be written as

$$R = \frac{\bar{u}}{a\omega\cos\theta} = \frac{2(\Delta s)^2}{a^2\pi^2}\left[\left(\frac{\Delta s}{L}\right)^2 + 4\ell^2\left(\frac{\Delta s}{W}\right)^2\right]^{-1}. \tag{7.3}$$

The quantity on the left-hand side of (7.3) is the ratio of the fluid's relative velocity to the absolute velocity of the obstacle at latitude θ. We shall refer to this ratio R as the kinematic Rossby number after Long, Fultz and Frenzen (loc. cit.). Since the center of the obstacle is located at 45°N, we chose $\theta = 45^{\circ}$. Using the numerical values (5.1) as discussed in section 5, we calculated the values of R for various values of ℓ as listed in Table 2(a). On the other hand, in Table 2(b), we show the corresponding values of R for the three westerly cases of $\bar{u}$ = 8, 20 and 40 m/sec and observed number of waves in each case.

Table 2

(a) Theoretical relation between the number of waves ℓ and the kinematic Rossby number R ($= \bar{u} / (\omega a \cos 45°)$) as computed from (7.3).

(b) Observed relation between ℓ , R and initial westerly speed $\bar{u}$

a. Theoretical		b. Observed		
ℓ	R	ℓ	R	$\bar{u}$ (m/s)
1	0.200			
2	0.125	2	0.122	40
3	0.0769	3-4	0.0611	20
4	0.0500			
5	0.0345			
6	0.0250	5-6	0.0244	8
7	0.0189			
8	0.0147			

In Figure 10, the ordinate, ℓ , shows the number of waves plotted against the various values of the kinematic Rossby number R , (abscissa) as shown in Table 2(a). The vertical arrows show the observed ranges of ℓ for a given value of R as listed in Table 2(b). The general agreement between the observed and theoretical values indicates that the waves produced by the obstacle

are indeed the "planetary" waves of Rossby-Haurwitz type. Long, Fultz and Frenzen (loc. cit.) found also in their laboratory experiments discussed in the Introduction, that the observed number of waves agrees with the numbers expected from the stationary Haurwitz wave formula (Haurwitz, 1940b). It is interesting to note a general agreement between the results of the laboratory experiments and the present numerical experiments in spite of simplifications introduced in the numerical model.

Next we shall attempt to give an explanation of why the differences exist between the characteristics of the westerly and easterly flows past the obstacle as observed in the numerical experiments. In the steady state, (7.1) reduces to

$$\nabla^2 h + \frac{\beta}{\bar{u}} h = -\lambda^2 H . \tag{7.4}$$

The solutions of equations similar to (7.4) have been discussed by Stewart (1948), Charney and Eliassen (1949), Bolin (1950) and others. However, these authors studied only the case of $\bar{u} > 0$, westerly flows. Here we shall consider a more general case including $\bar{u} < 0$, easterly flows. To simplify the analysis, it is assumed that the channel is extended to the plus and minus infinity in the x-direction taking the origin of the coordinate at the center of the mountian.

The boundary conditions are that (1) h must vanish at $y = W/2$ and $y = -W/2$, and (2) h remains finite at $x = \pm\infty$. Because of the condition (1), it is convenient to expand h and H in terms of Fourier series. We set

$$h(x,y) = \sum_{r=1}^{\infty} \phi_r(x) \cos\left(\frac{r\pi}{W} y\right) \tag{7.5a}$$

$$H(x,y) = \sum_{r=1}^{\infty} \Phi_r(x) \cos\left(\frac{r\pi}{W} y\right) \tag{7.5b}$$

where ϕ_r is to be computed and

$$\Phi_r(x) = -\frac{2\lambda^2}{W} \int_{-W/2}^{W/2} H(x,\eta) \cos\left(\frac{r\pi}{W}\right) \eta \, d\eta.$$

Substituting (7.5) into (7.4) we obtain an ordinary inhomogeneous equation for $\phi_r(x)$:

$$\frac{d^2\phi_r}{dx^2} + \sigma \phi_r = \Phi_r(x) \tag{7.6}$$

where $$\sigma = \frac{\beta}{\bar{u}} - \left(\frac{r\pi}{W}\right)^2.$$

This equation with the boundary condition (2) can be solved using a standard method. Once ϕ_r is computed, $h(x,y)$ may be expressed in the following form:

$$h(x,y) = \int_{-\infty}^{\infty} d\xi \int_{-w/2}^{w/2} H(\xi,\eta)\, G(x,y|\xi,\eta)\, d\eta \tag{7.7}$$

where $G(x,y|\xi,\eta)$ is the Green's function which is given as follows:

Class 1, $\sigma > 0$.

$$G(x,y|\xi,\eta) = -\frac{2\lambda^2}{w} \sum_{r=1}^{\infty} \frac{\cos\left(\frac{r\pi}{w}\right)\eta \cos\left(\frac{r\pi}{w}\right)y}{\sigma(r)} \times \sin\left\{\sqrt{\sigma(r)}\ (x-\xi)\right\}. \tag{7.8}$$

The form of the Green's function suggests that (7.7) is a wave-like solution.

Class 2, $\sigma < 0$.

$$G(x,y|\xi,\eta) = \frac{\lambda^2}{w} \sum_{r=1}^{\infty} \frac{\cos\left(\frac{r\pi}{w}\right)\eta \cos\left(\frac{r\pi}{w}\right)y}{|\sigma(r)|} \times \exp\left\{\pm\sqrt{|\sigma(r)|}\ (x-\xi)\right\} \tag{7.9}$$

where the plus sign is for $x < \xi$ and the minus is for $x > \xi$. The form of the Green's function indicates that (7.7) shows an exponentially decaying solution.

The case of easterly flows, $\bar{u} < 0$, falls into Class 2. The distance D defined by

$$D = \left\{ \left(\frac{r\pi}{W}\right)^2 + \frac{\beta}{|\bar{u}|} \right\}^{-1/2}$$

denotes the horizontal scale in the x-direction for which the Green's function (7.9) decreases by the factor of e^{-1} (=0.3679). To evaluate the magnitude of D , let us assume $r = 1$, which corresponds to a simple-mode solution in the y-direction. For the following numerical values,

$$W = 18\Delta S = 393.073 \text{ Km} \times 18$$
$$\beta = 1.6145 \times 10^{-11} \text{ m}^{-1}\text{sec}^{-1} \quad (\text{at } 45^\circ N) \tag{7.10}$$

the values of $D's$ for various intensities of $\bar{u}$ are listed in Table 3.

Table 3

The values of D'_s against various values of $\bar{u}$.

$\bar{u}$ (m/s)	40	30	20	10
D (km)	1290	1166	998	743

It is seen from Table 3 that the intensity of perturbation decreases by a factor of e^{-1} within a distance of about 1000 km. This result suggests that the modification of flow, due to the presence of an

obstacle in easterly flows, affects only the vicinity of the obstacle which is in agreement with the result of Case C in Section 6.

In the case of westerly flows, $\bar{u} > 0$, the solution (7.7) falls into either Class 1 or Class 2 according to

$$r \begin{matrix} < \\ > \end{matrix} r_c \qquad \begin{matrix} \text{Class 1} \quad \text{(wave type)} \\ \text{Class 2} \quad \text{(decaying type)} \end{matrix} \tag{7.11}$$

where $r_c = \frac{W}{\pi}\sqrt{\frac{\beta}{\bar{u}}}$, the critical modal number which is derived by setting $\sigma = 0$. Table 4 shows the value of r_c for various intensities of $\bar{u}$ and the numerical data (7.10). A relationship similar to (7.11) was also pointed out by Magata (1957).

Table 4

The critical modal number r_c versus $\bar{u}$.

r_c	1	2	3	4	5
$\bar{u}$ (m/s)	81.9	20.5	9.1	5.1	3.3

The inequality (7.11) indicates that the perturbations whose modal number is larger than r_c are not of wave type, but of exponentially decaying type. From Table 4, it is seen that for $\bar{u}$ = 40 m/sec, only the perturbations with a single mode in the y-direction are expected to appear as wave type (as observed in Case A in Section 6). On the other hand, for $\bar{u}$ = 8 m/sec, the perturbations with one, double and triple modes can appear as wave type solutions, and therefore the development of a small-scale pattern in the y-direction can be expected (as observed in Case D).

7. Conclusions

The study was made to clarify the dynamical effect of the earth's topography upon the large-scale motion of the atmosphere. The model is based upon the barotropic equations in Eulerian form. The results of the numerical integrations demonstrate that:

(1) The use of the stationary solutions (3.1) as the initial conditions of the problem yields quasi-geostrophic motions in the presence of mountains in the model.

(2) Westerly flows past the circular mountain produced a train of long waves on the lee side of the mountain. If the latitudinal variation of the Coriolis parameter is neglected (in the case of the tangent plane approximation), such a train of waves does not appear.

(3) The characteristics of the long waves found in (2) are identified as "planetary" waves. The number of waves generated in the westerly cases agrees with the number expected from the steady-state Rossby-Haurwitz wave formula for various intensities of the zonal flow past the mountain.

(4) Easterly flows past the mountain do not generate a train of long waves. The characteristic differences between westerly and easterly flows past an obstacle are explained based upon the Green's function solutions of the steady-state linearized equations of the model.

The meteorological implications of the present results will be discussed in a separate article.

Acknowledgments

The author wishes to thank Prof. Dave Fultz, University of Chicago, for his permission to reproduce in this article the picture of the apparatus of the rotating hemispherical shells.

The programming for the CDC 3600 was assisted by Bernard O'Lear.

References

Asai, T. and T. Nitta, 1963: Numerical test of the finite-difference form of the primitive equations for a barotropic model including orography. Papers in Meteorology and Geophysics, 14, 1 - 11.

Belousov, S. L., and V. V. Bykov, 1957: On the calculation of the influence of mountains in the forecast of a baric field (in Russian). Izv. Akad. Nauk USSR, Ser. Geofiz., No. 9, 1142 - 1153.

Bolin, B., 1950: On the influence of the earth's orography on the general character of the westerlies. Tellus, 2, pp. 184 - 195.

Boyko, A. P., 1963: Hydrodynamic forecasting of pressure fields in the mid-level of the atmosphere for the entire sphere of the earth, taking orography into consideration (in Russian). Doklady Akademii Nauk USSR, Moscow, 153, (6), 1303 - 1306.

Charney, J. G. and A. Eliassen, 1949: A numerical method for predicting the perturbations of the middle latitude westerlies. Tellus, 1, (2), pp. 38 - 54.

Frenzen, P., 1955: Westerly flow past an obstacle in a rotating hemispherical shell. Bull. Amer. Meteorol. Soc. 36, (5), pp. 204 - 210.

Fultz, D. and R. R. Long, 1951: Two-dimensional flow around a circular barrier in a rotating spherical shell. Tellus, 3, pp. 61 - 68.

Fultz, D. and P. Frenzen, 1955: A note on certain interesting ageostrophic motions in a rotating hemispherical shell. Journal of Meteorology, 12, pp. 332-338.

Gambo, K., 1956: The topographical effect upon the jet stream in the westerlies. Journal of Meteorological Society of Japan, 34, 24 - 28.

Gambo, K., 1957: The scale of atmospheric motions and the effect of topography on numerical weather prediction in the lower atmosphere. Papers in Meteorology and Geophysics, 8, (1), 1 - 24.

Haurwitz, B., 1940a: The motion of atmospheric disturbances. Journal of Marine Research, 3, 35 - 50.

Haurwitz, B., 1940b: The motion of atmospheric disturbances on the spherical earth. Journal of Marine Research, 3, 254 - 267.

Houghton, D., A. Kasahara and W. Washington, 1965: Long-term integration of the barotropic equations in Eulerian form. National Center for Atmospheric Research, Boulder Colorado, To be submitted to Monthly Weather Review

Kawata, Y., 1957: The influence of the Rocky Mountains on non-steady isobaric height patterns. Journal of Meteorological Society of Japan, 35, 174 - 183.

Kibel, I. A., 1957: An Introduction to the Hydrodynamical Methods of Short Period Weather Forecasting (in Russian). (See Section 11.1 and 11.2) MacMillan Co.

Lax, P. D. and B. Wendroff, 1960: Systems of conservation laws. Communication on Pure and Applied Mathematics, 13, 217 - 237.

Long, R. R., 1952: The flow of a liquid past a barrier in a rotating spherical shell. Journal of Meteorology, 9, 187 - 199.

Magata, M., 1957: On the topographical effect upon the perturbations of the middle latitude westerlies. Papers in Meteorology and Geophysics, 8, 25-38.

Murakami, T., 1956: The topographical effect upon the stationary upper flow patterns. Papers in Meteorology and Geophysics, 7, 69 - 89.

Musaelyan, Sh. A., 1960: Planetary orographic waves in the westerly flows (in Russian). Collected papers on Problems of Dynamic Meteorology, Inst. Applied Geophysics, Moscow, pp 21-54

Phillips, N. A., 1963: Geostrophic motion. Reviews of Geophysics, 1, (2) 123 - 176.

Richtmyer, R. D., 1963: A survey of difference methods for non-steady fluid dynamics. Technical Notes No. 2, pp. 25. National Center for Atmospheric Research, Boulder, Colorado

Rossby, C.-G. and Collaborators, 1939: Relation between variations in the intensity of the zonal circulation of the atmosphere and the displacements of the semi-permanent centers of actions. Journal of Marine Research, 2, 38 - 55.

Rossby, C.-G., 1949: Dispersion of planetary waves in a barotropic atmosphere, Tellus, 1, 54 - 58.

Stewart, H. J., 1948: A theory of the effect of obstacles on the waves in the westerlies. Journal of Meteorology, 5, 236 - 238.

Fig. 1: The rotating hemispherical shells for studying two-dimensional motions of homogeneous fluid around an obstacle used by Fultz, Long and Frenzen.

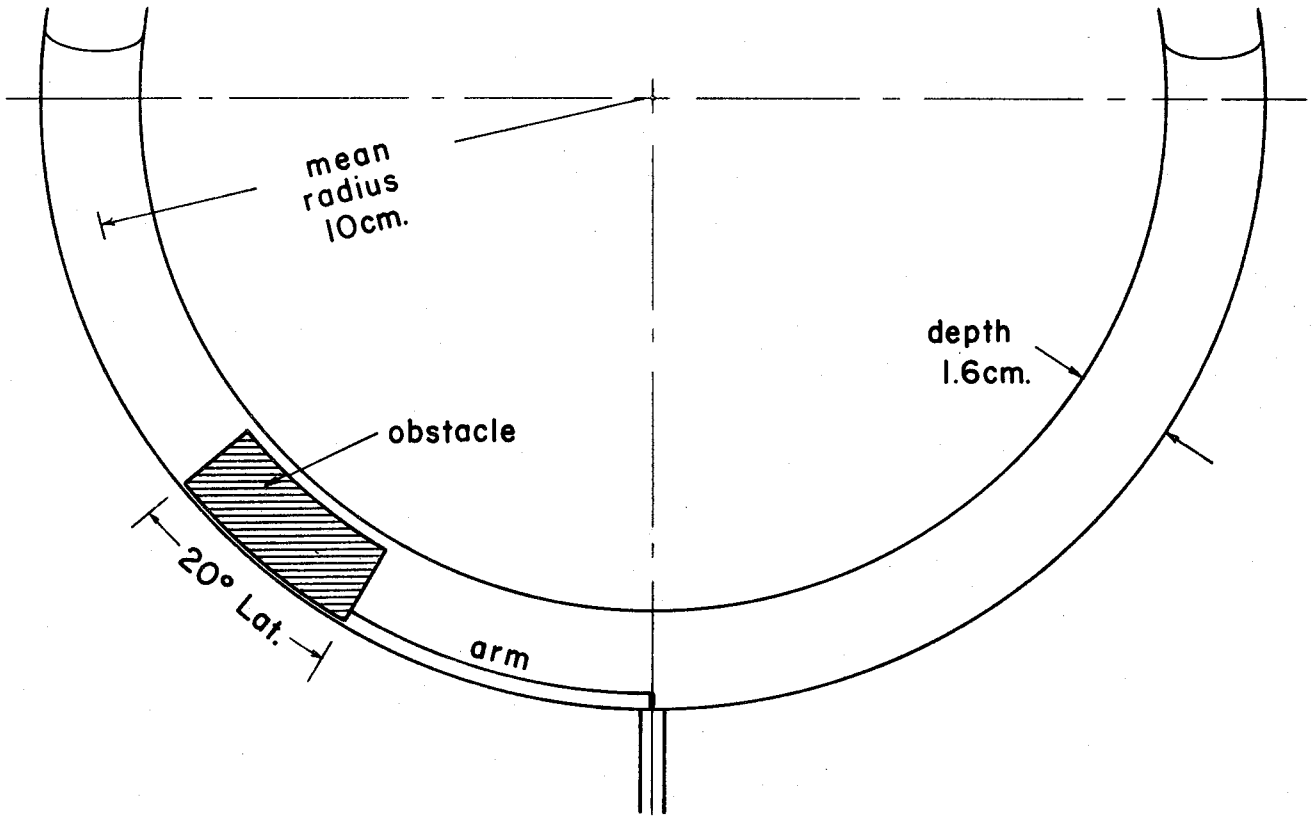

Cross Section of Spherical Shell With Obstacle.

Fig. 2: A cross section view of the shells and the position of the obstacle.

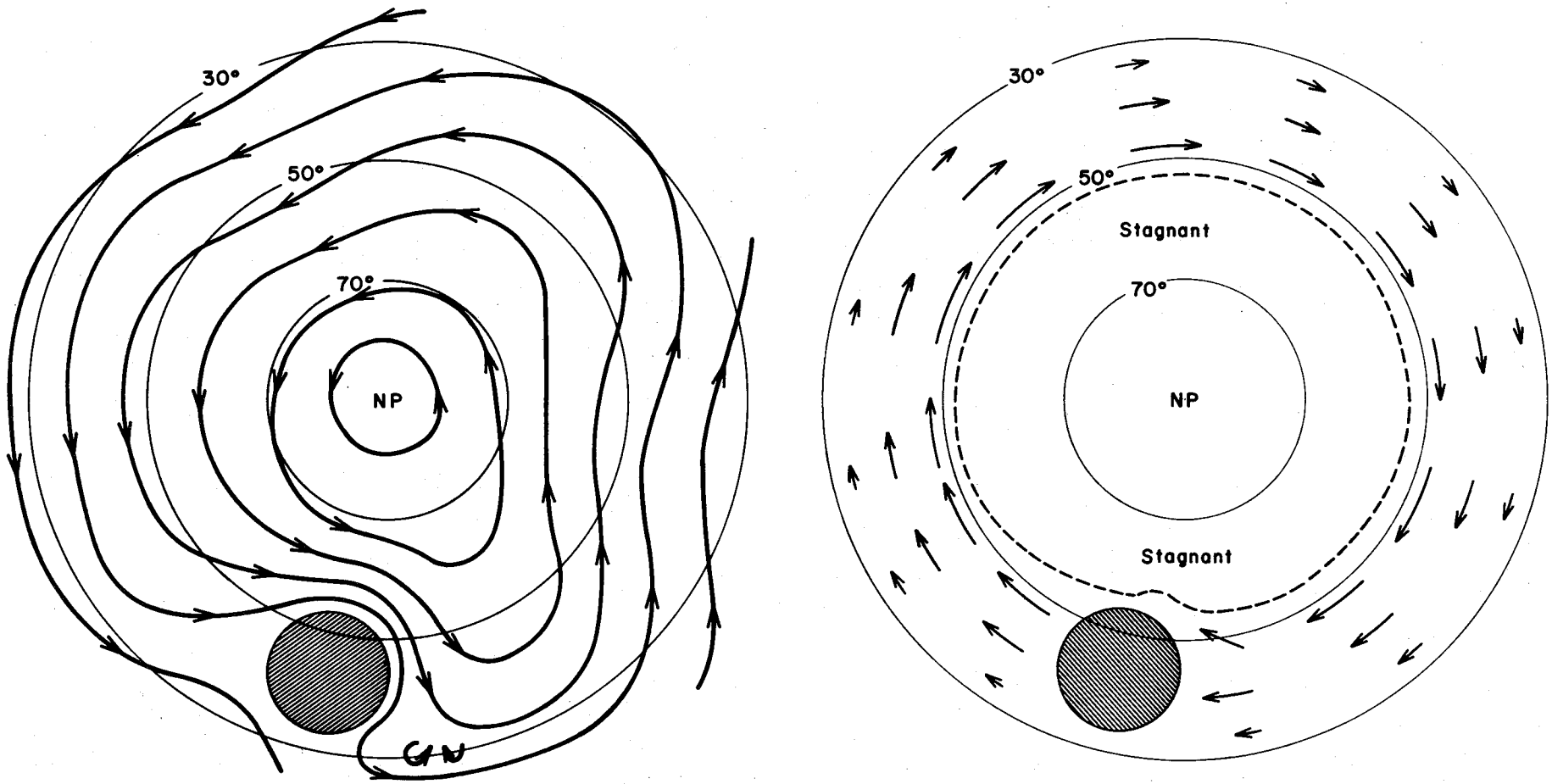

Westerly Case **Easterly Case**

Fig. 3: Two schematic sketches of the flow patterns observed relative to the obstacle. Left: Westerly flow case. Right: Easterly flow case. Notice the remarkable differences between the two patterns. (After Fultz, Long and Frenzen.)

Model

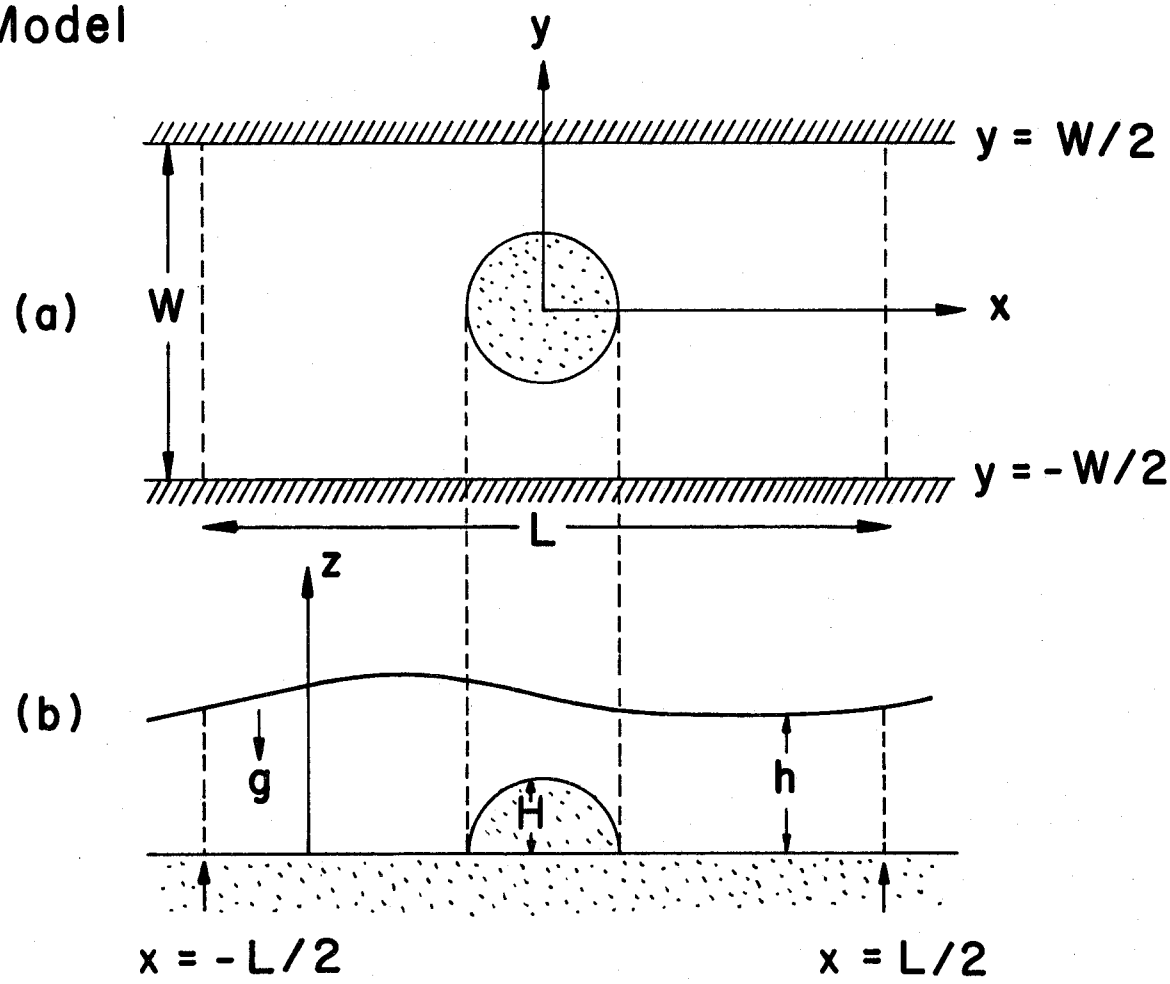

Equations

$$\frac{\partial u}{\partial t} + u\frac{\partial u}{\partial x} + v\frac{\partial u}{\partial y} = -g\frac{\partial h}{\partial x} + fv$$

$$\frac{\partial v}{\partial t} + u\frac{\partial v}{\partial x} + v\frac{\partial v}{\partial y} = -g\frac{\partial h}{\partial y} - fu$$

$$\frac{\partial h}{\partial t} + \frac{\partial}{\partial x}\{u(h-H)\} + \frac{\partial}{\partial y}\{v(h-H)\} = 0$$

$$t: \text{time}, \quad u = \frac{dx}{dt}, \quad v = \frac{dy}{dt}$$

Fig. 4: (a) The bird's-eye view of the flow. A circular obstacle is at the center of the domain. (b) The cross section view of the flow.

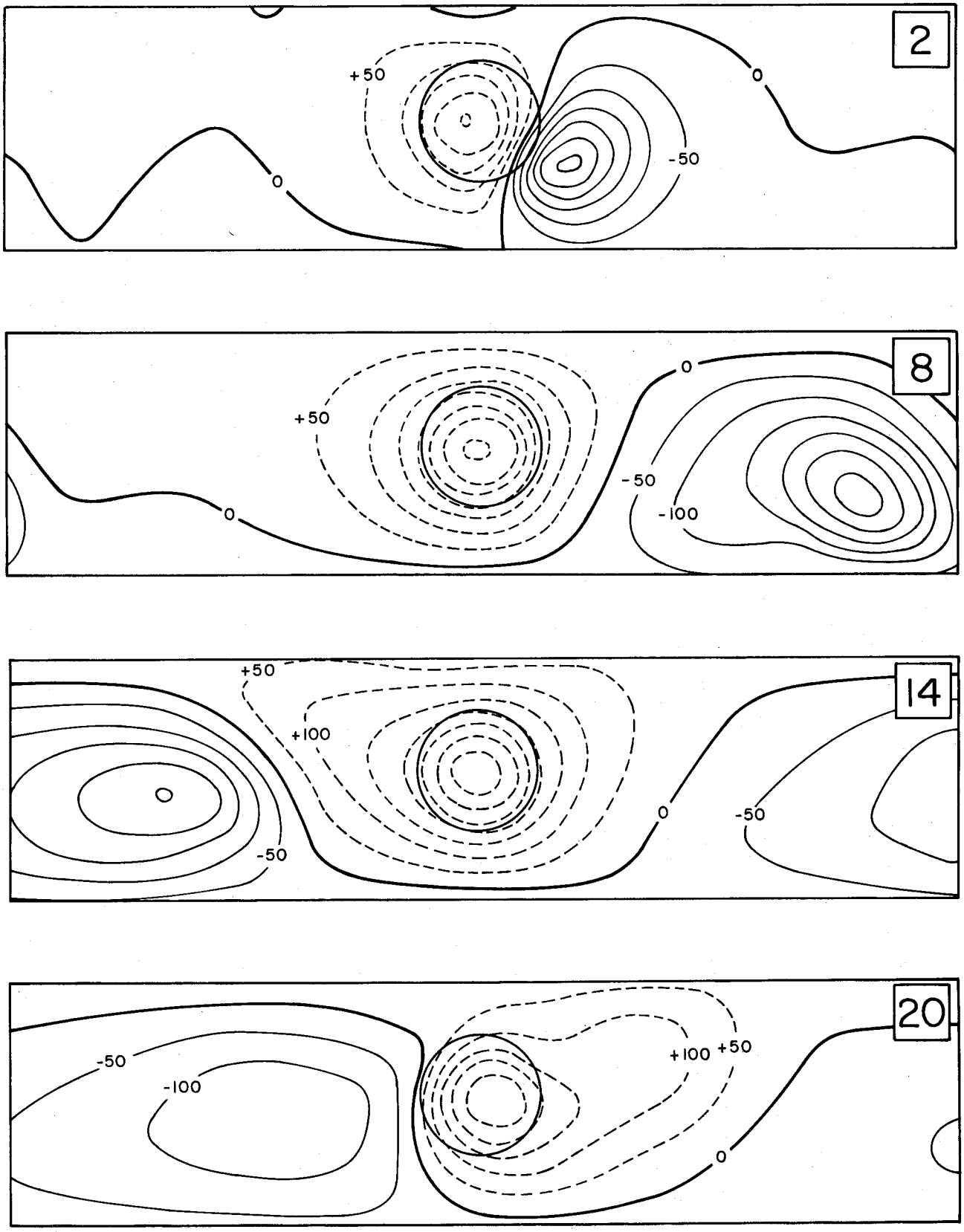

Constant f, U = 20 m/s

Fig. 5: Evolution of height deviation field for Case A. Time, in days, is given in upper right corner of each chart. Circular obstacle is indicated by the circle. Contours are drawn every 50 meter interval.

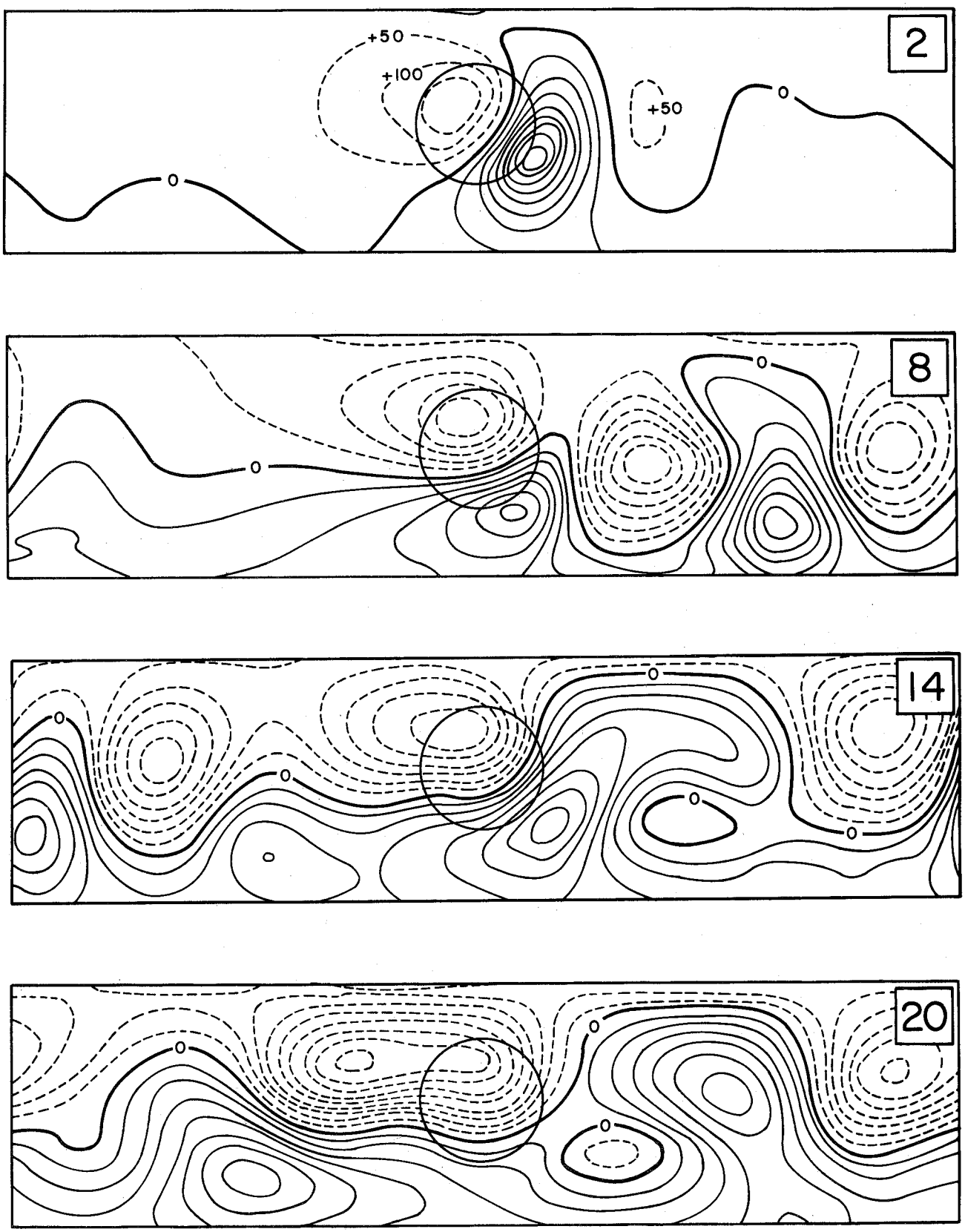

Variable f, U = 20 m/s

Fig. 6: Evolution of height deviation field for Case B. Notice remarkable differences between the two Cases A and B.

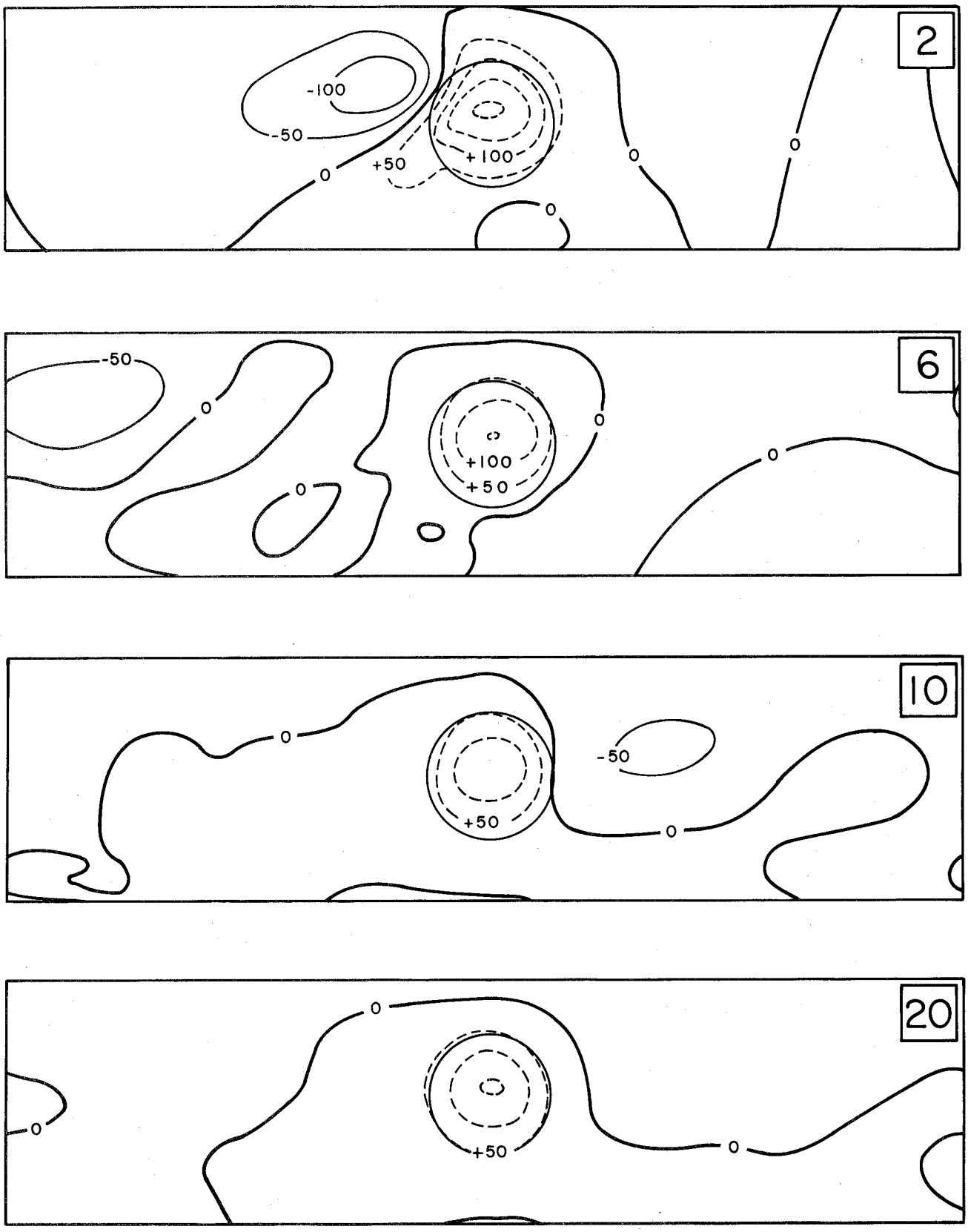

Variable f, U = - 20 m/s (easterly case)

Fig. 7: Evolution of height deviation field for Case C. Observe remarkable differences between Cases B and C.

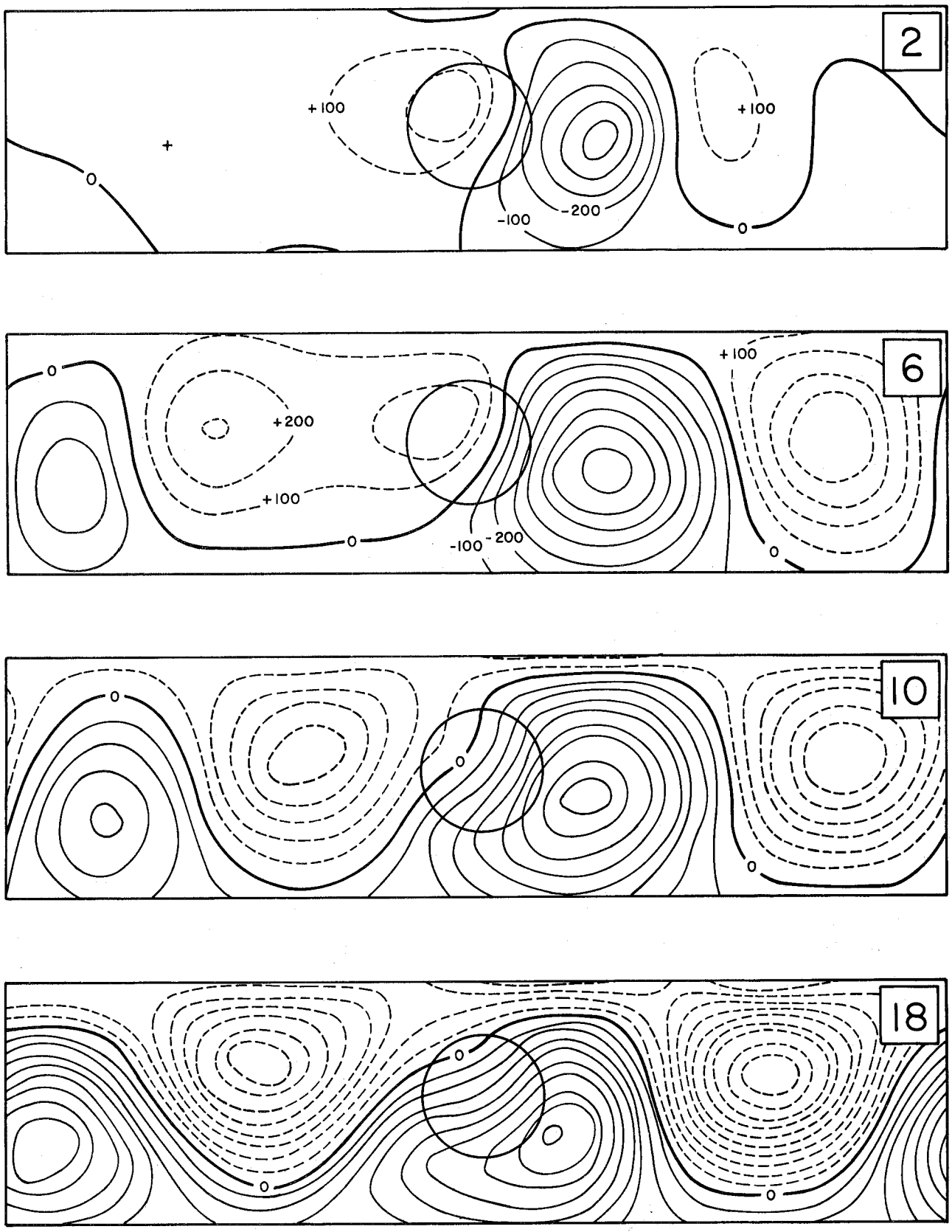

Variable f , U = 40 m/s

Fig. 8: Evolution of height deviation field for Case D. Contours in this case are drawn every 100 meter interval.

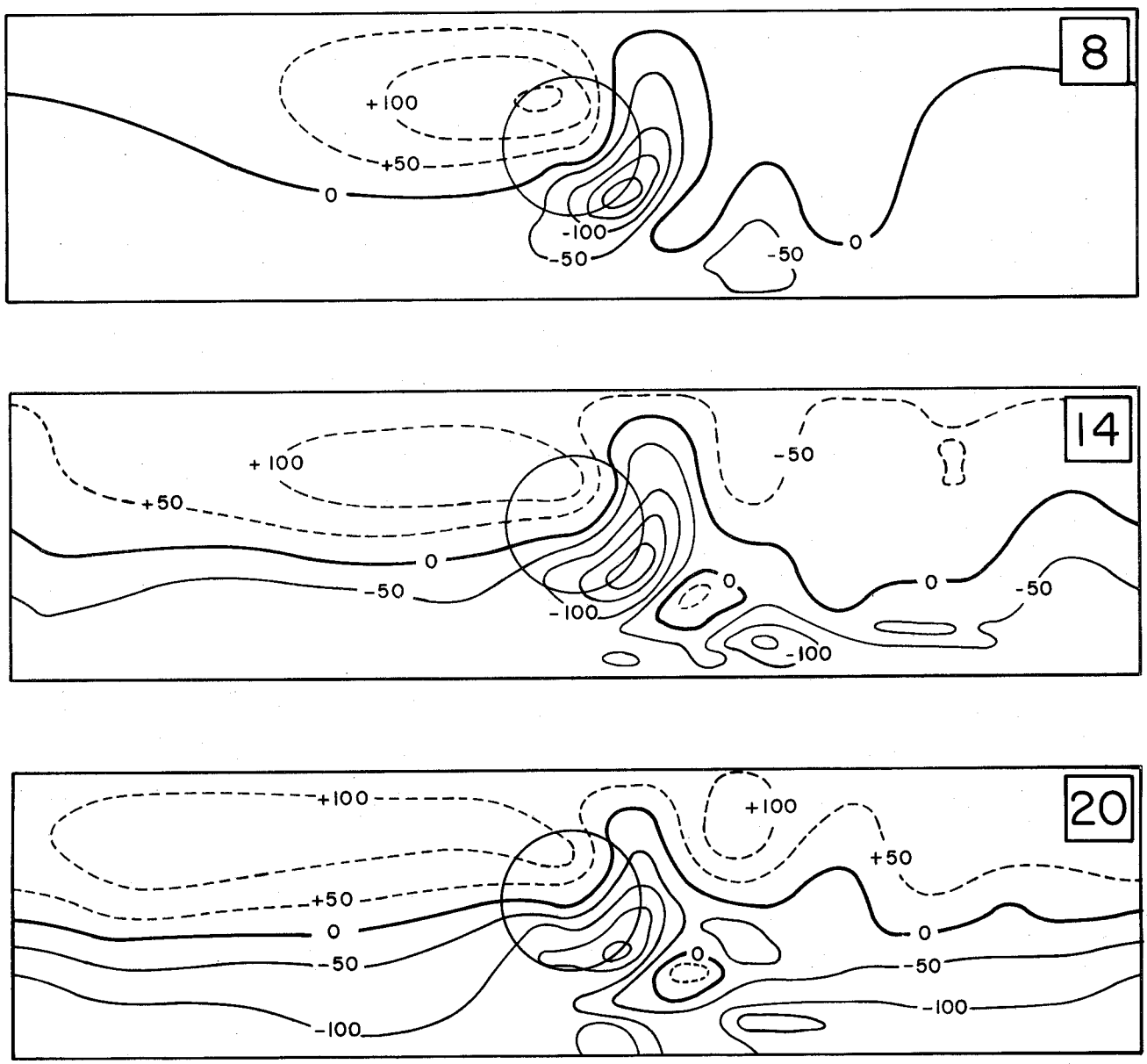

y - Component of Velocity

Fig. 9: Evolution of height deviation field for Case E. The fourth figure shows the pattern for the y-component of velocity at 20 days.

A

Theoretical	
ℓ	R
1	0.200
2	0.125
3	0.0769
4	0.0500
5	0.0345
6	0.0250
7	0.0189
8	0.0147

B

Observed		
ℓ	R	$\bar{u}$
2	0.122	40
3-4	0.0611	20
5-6	0.0244	8

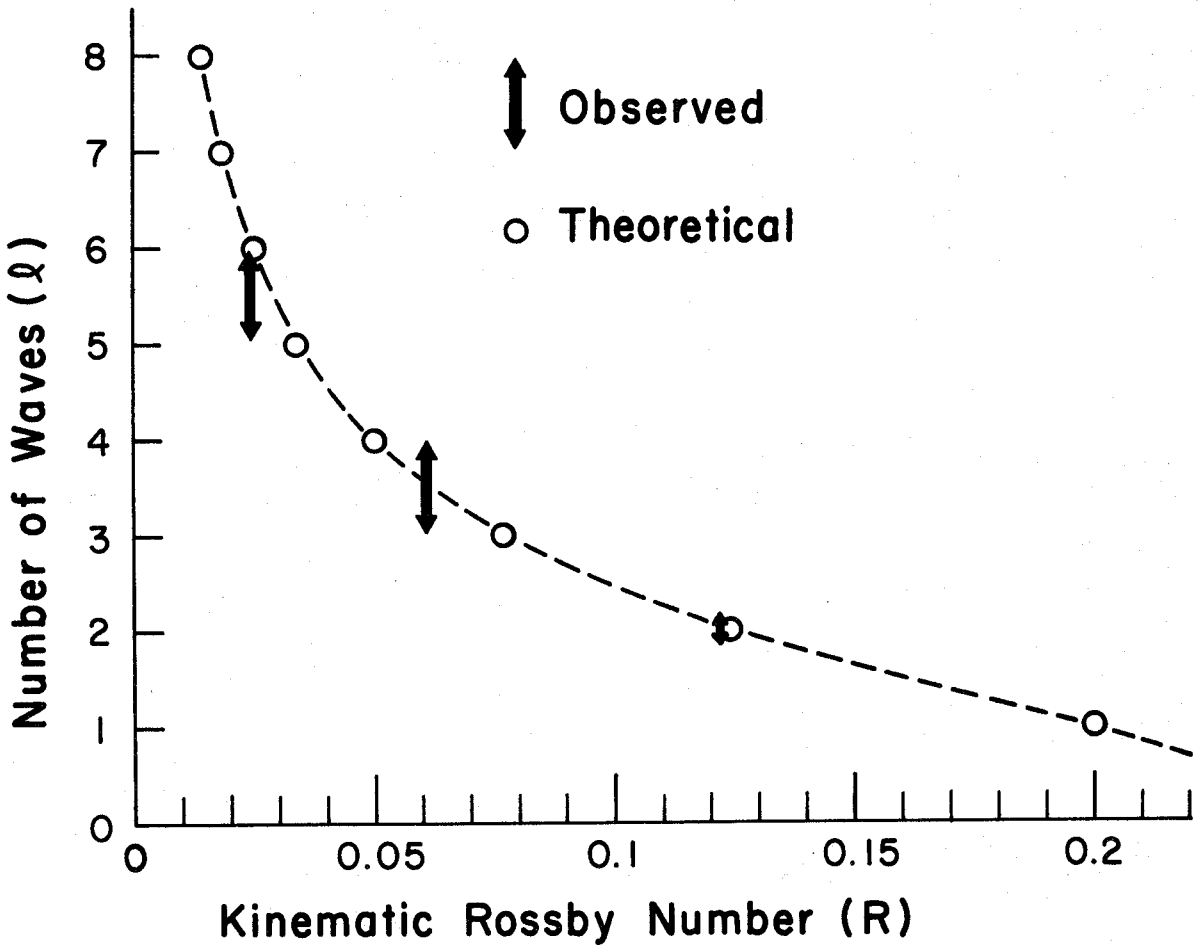

Fig. 10: Number of waves, ℓ, plotted against kinematic Rossby number R as shown in Table 1(a). Vertical arrows show the observed ranges of ℓ for a given value of R as listed in Table 1(b).